

---

# Scaling Hot-Electron Generation to High-Power, Kilojoule-Class Laser–Solid Interactions

High-intensity laser–solid interactions ( $>10^{18}$  W/cm<sup>2</sup>) accelerate large numbers of thermal electrons to relativistic energies. These high-energy, MeV-scale electrons are a source of significant energy deposition within plasmas and are used extensively in plasma-based particle acceleration,<sup>1–3</sup> creation of warm dense matter,<sup>4</sup> laboratory high-energy astrophysics,<sup>5</sup> ultrafast  $\gamma$ -ray generation,<sup>6</sup> and fast-ignition research.<sup>6,7</sup> Efficient hot-electron generation is of great importance for the energetic feasibility of these applications and has been studied intensively.<sup>6,8–17</sup>

Previous solid-target experiments showed energy-conversion efficiencies into hot electrons ( $\eta_{L\rightarrow e}$ ) of up to several tens of percent for picosecond or shorter pulses of 1- $\mu$ m light and laser intensities from  $10^{18}$  W/cm<sup>2</sup>  $\leq I \leq 10^{20}$  W/cm<sup>2</sup> (Refs. 6,8–17). With recent developments in laser technology, it is now possible to generate kilojoule-class,  $\tau_p = 10$ -ps pulses that can be focused to intensities of  $I > 10^{18}$  W/cm<sup>2</sup> (Ref. 18). Such long-duration, high-intensity laser pulses hold great promise for high-energy applications that require rapid electron-energy deposition over time scales that are short compared to the typical hydrodynamic decompression times of solid and laser-compressed targets.

In fast ignition, laser-compressed deuterium and tritium are rapidly heated and ignited by a high-intensity laser pulse.<sup>6,7</sup> An intense, multikilojoule, 10- to 20-ps-long laser pulse is required to generate the ignition spark with optimal electron-beam energies and currents for energy deposition within the fuel assembly. Knowledge of the coupling of a high-intensity laser into energetic electrons that heat the fuel, in addition to how this scales to ignition-class lasers, is critical to understanding spark generation and fast ignition.

Hot-electron generation in this regime is only partially understood, however, particularly at high laser energies ( $E_L > 1000$  J) and long laser-pulse durations ( $\tau_p \sim 10$  ps), where no previous data exist because of the unavailability of suitably high-energy lasers. With increasing laser-pulse duration, a number of processes affect energy coupling to solid targets,

including pre-plasma formation,<sup>19,20</sup> electron transport,<sup>21</sup> hole boring,<sup>22</sup> and laser-driven shock formation.<sup>23</sup> Understanding these effects on energy coupling is crucial for scaling hot-electron generation to long-pulse, high-intensity lasers. Definitive measurements of the effect of laser-pulse duration on  $\eta_{L\rightarrow e}$  are reported in this article.

X-ray spectroscopic measurements of hot-electron generation in high-intensity laser–solid interactions show that the conversion efficiency is independent of laser-pulse duration. Thin-foil targets have been heated with hot electrons generated by  $\tau_p = 10$ -ps pulses focused to intensities of  $I > 10^{18}$  W/cm<sup>2</sup>, and  $\eta_{L\rightarrow e}$  has been inferred with K-photon spectroscopy. Comparing the energy emitted in K photons to target-heating calculations shows an energy-coupling efficiency to hot electrons of  $\eta_{L\rightarrow e} \sim 20\%$  with laser powers from  $1 \text{ TW} \leq P_L \leq 210 \text{ TW}$ . These are the first experiments to study hot-electron generation with intense,  $\tau_p = 10$ -ps pulses at such high laser powers. Time-resolved x-ray emission measurements suggest that hot electrons are generated over the entire duration of the incident laser drive. The K-photon emission data are compared to other published data at similar laser intensities, showing for the first time that  $\eta_{L\rightarrow e}$  is independent of laser-pulse duration from  $1 \text{ ps} \leq \tau_p \leq 10 \text{ ps}$ .

The experiments were carried out using LLE’s Multi-Tera-watt (MTW)<sup>24,25</sup> and Omega EP<sup>18</sup> Laser Facilities. For these experiments, the MTW laser delivered an energy of  $E_L = 10$  J in a  $\tau_p = 10$ -ps pulse at a wavelength of  $\lambda_L = 1.054 \mu\text{m}$ . The laser pulse was focused by an  $f/3$ , off-axis parabolic mirror at normal incidence to the target with an  $R_{80} = 5 \mu\text{m}$ , where  $R_{80}$  is the spot radius containing 80% of the laser energy, providing a laser intensity of  $I = 1 \times 10^{18}$  W/cm<sup>2</sup>. OMEGA EP delivered higher laser energies from  $300 \text{ J} \leq E_L \leq 2100 \text{ J}$  in a  $\tau_p = 10$ -ps pulse at a wavelength of  $\lambda_L = 1.054 \mu\text{m}$ . An  $f/2$ , off-axis parabolic mirror focused the laser pulse at either  $45^\circ$  or normal incidence to the target with an  $R_{80} = 25 \mu\text{m}$ , providing laser intensities of up to  $I \sim 10^{19}$  W/cm<sup>2</sup>. The targets were Cu foils with dimensions that were varied between  $600 \times 600 \times 50 \mu\text{m}^3$  and  $75 \times 75 \times 3 \mu\text{m}^3$ , mounted on a 17- $\mu$ m-thick silicon-carbide stalk.

Pre-plasma expansion prior to intense laser irradiation affects the energy coupling to solid targets,<sup>19,20</sup> particularly at high laser energies, and is caused by low laser contrast. For these OMEGA EP shots, fast-diode measurements indicate that the laser pedestal typically reaches  $6 \times 10^{-7}$  of the peak laser power and contains  $10^{-4}$  of the total laser-pulse energy. For the experiments reported here, the energy contained in the pedestal varied from  $40 \text{ mJ} \leq E_{\text{ped}} \leq 210 \text{ mJ}$ . Over this energy range, calculations made using the 1-D radiation hydrodynamic code *LILAC*<sup>26</sup> indicate that the pre-plasma extends up to 5 to  $10 \mu\text{m}$  between the critical- and the solid-density plasma.

The main diagnostic for measuring K-photon emission from the target was an absolutely calibrated, single-photon-counting x-ray spectrometer based on an SI-800 x-ray charge-coupled device.<sup>27</sup> A combination of heavy shielding and collimation, and a large target-to-spectrometer distance, reduces the number of Cu K-photon hits that are detected, satisfying the single-photon-counting regime, while reducing the hard x-ray flux. Cu filters that transmit Cu  $K_{\alpha}$  and  $K_{\beta}$  photons below the filter K edge further optimize the signal to background of the measured spectrum. A graphite (HOPG) crystal spectrometer provided a complementary measurement of the K-photon yield.<sup>28</sup> The radiation emission time was measured using an ultrafast x-ray streak camera with a temporal resolution of about 2 ps (Ref. 29).

Typical K-photon spectra obtained in the experiment are shown in Fig. 124.13. Figure 124.13(a) shows a time-integrated x-ray emission spectrum from a  $500 \times 500 \times 20\text{-}\mu\text{m}^3$  Cu target irradiated with an  $E_L = 1000\text{-J}$ ,  $\tau_p = 10\text{-ps}$  pulse. Figure 124.13(b) shows an x-ray emission spectrum from a  $75 \times 75 \times 5\text{-}\mu\text{m}^3$  Cu target irradiated with the same laser conditions.

The emission spectra show peaks at 8.05 keV and 8.91 keV, where the Cu plasma emits  $K_{\alpha}$  and  $K_{\beta}$  inner-shell radiation. As hot electrons move through the target, the atomic electrons in the 1s shell of copper ions are ejected by electrons with energies 2 to  $3 \times$  the copper K-shell ionization potential ( $\sim 20$  to 25 keV). During de-excitation, the system relaxes to a lower-energy state, with  $2p \rightarrow 1s$  and  $3p \rightarrow 1s$  transitions generating  $K_{\alpha}$  and  $K_{\beta}$  photons. The emission lines are fit to Gaussian line shapes with a full width at half maximum (FWHM) of 220 eV. The emission spectra contain the thermal  $\text{He}_{\alpha}$  and  $\text{Ly}_{\alpha}$  ionic-line emission that is generated from hot surface plasma on the laser-irradiated side of the target.

The main observation from these measurements is the suppressed K-photon yield from the reduced-mass target.

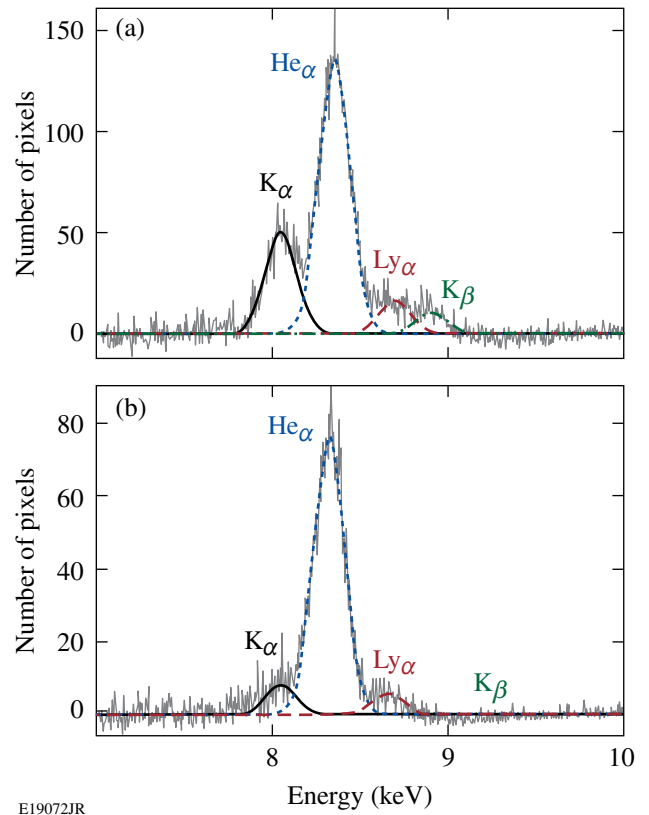


Figure 124.13 Comparison of K-photon emission spectra from (a)  $500 \times 500 \times 20\text{-}\mu\text{m}^3$  and (b)  $75 \times 75 \times 5\text{-}\mu\text{m}^3$  Cu targets irradiated with  $E_L = 1000\text{-J}$ ,  $\tau_p = 10\text{-ps}$  laser pulses.

The  $75 \times 75 \times 5\text{-}\mu\text{m}^3$  Cu target generates no  $K_{\beta}$  radiation and has a dramatically suppressed  $K_{\alpha}$  yield compared to the larger-volume target. The suppressed K-photon yield suggests higher-energy-density conditions and high thermal-electron temperatures in the reduced-mass target. This is expected for these high-energy interaction conditions.<sup>15–17,30</sup>

The method for calculating  $\eta_{L \rightarrow e}$  involves comparing K-photon emission from reduced-mass targets to target-heating calculations and was described previously in Ref. 16. It relies on a significant fraction of the laser-generated hot electrons being trapped by the target potential that develops because of the charge separation that occurs between the hot escaping electrons and the relatively immobile ions.<sup>12</sup> This effect has been studied theoretically<sup>16</sup> and confirmed experimentally.<sup>15,17,30</sup> The collisional range of MeV electrons in cold, solid-density copper is several hundred microns and is much greater than the target thickness used in the experiment (up to tens of microns). Hot electrons recirculate (reflux) throughout the target, efficiently transferring energy to the target material

until they range out. Capacitance model calculations indicate that hot-electron refluxing efficiencies in these targets reach >90%, making K-photon spectroscopy measurements of the contained hot electrons highly representative of  $\eta_{L \rightarrow e}$ .

Time-resolved x-ray emission measurements support the electron-refluxing interpretation for  $\tau_p = 10$ -ps pulses. Figure 124.14 shows the radiation time history for a  $100 \times 100 \times 10$ - $\mu\text{m}^3$  Cu target irradiated with an  $E_L = 1000$ -J,  $\tau_p = 10$ -ps pulse. The ultrafast x-ray streak camera was filtered as shown in Fig. 124.14 (inset), providing sensitivity to bremsstrahlung, inner-shell radiation, and thermal ionic-line emission.

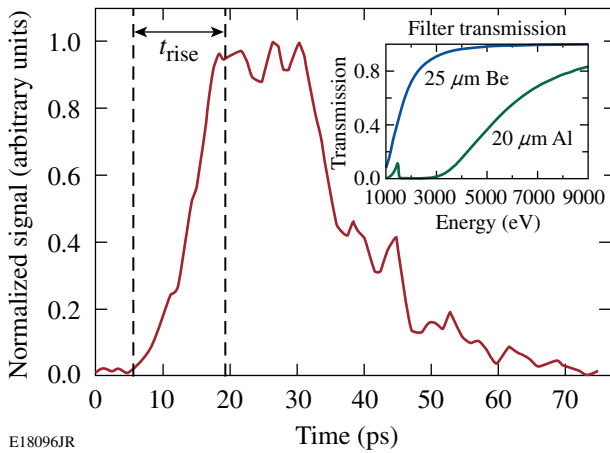


Figure 124.14  
Time-resolved x-ray emission from a  $100 \times 100 \times 10$ - $\mu\text{m}^3$  Cu target ( $E_L = 1000$  J,  $\tau_p = 10$  ps). The transmission functions for the x-ray streak-camera filters are shown (inset).

An increase in radiation emission correlated with the laser-pulse duration, implying an increasing hot-electron number density within the target over this period. This occurs because hot electrons reflux, suggesting constant laser-energy coupling to hot electrons over the entire duration of the incident laser drive. After the laser pulse ends, a radiation afterglow persists for around 20 ps (FWHM) and is likely a combination of inner-shell radiation and thermal radiation, emitted in response to the electron-energy deposition within the target. Thermal radiation persists until the hot electrons thermalize and target decompression dominates.

The absolute K-photon yield generated during the recirculation phase is sensitive to the time-varying number density of hot electrons within the target and target heating. The target-charging process governs the number of hot electrons contained

within the target, while target heating is caused mainly by electron–electron collisional energy deposition from the hot electrons. The ionization state of the target depends on collisions between bound and free conduction electrons. Once the thermal electron temperature inside the target exceeds a few hundred electron volts, the Cu M shell is depleted by thermal ionization, suppressing the plasma’s ability to generate  $K_\beta$  photons. Several hundreds of electron volts are required to deplete the Cu L shell. Time-integrated K-photon emission measurements quantify the target heating, making it possible for  $\eta_{L \rightarrow e}$  to be inferred by comparison to target-heating calculations, which are used to predict the ratio of  $K_\beta$  to  $K_\alpha$  ( $K_\beta/K_\alpha$ ) for a given hot-electron conversion efficiency.

The data show that suppression of the K-photon yield is governed by target energy density. Figure 124.15 shows the experimentally measured values for  $(K_\beta/K_\alpha)$  from reduced-mass targets plotted as a function of the ratio of the laser energy to the target volume (in units of  $\text{J}/\text{mm}^3$ ). The data obtained with 10-ps pulses (blue data points) are compared to previously published data with 1-ps pulses (black data points).<sup>17</sup> The measured values for  $K_\beta/K_\alpha$  are normalized to those measured from Cu foils when target heating is negligible ( $K_\beta/K_\alpha \sim 0.14$ ).

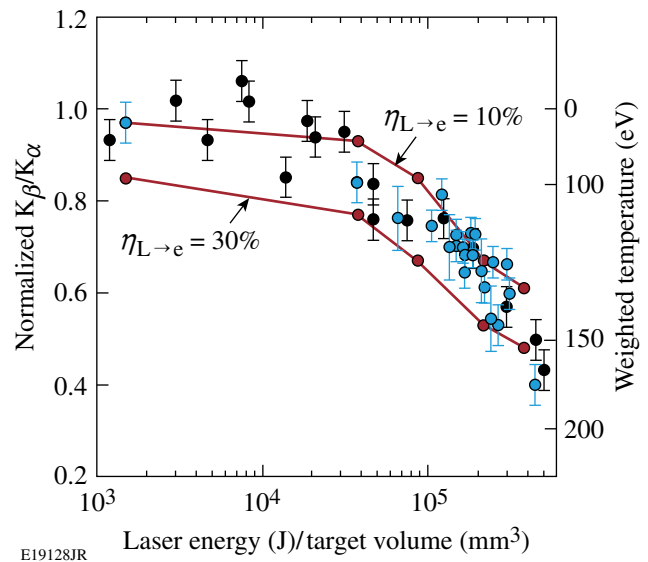


Figure 124.15  
Experimental  $K_\beta/K_\alpha$  data [normalized to the cold-material value (left axis)] and inferred bulk-electron temperature (right axis) as a function of laser energy (J)/target volume ( $\text{mm}^3$ ). Data for 10-ps pulses (blue) and 1-ps pulses (black reproduced from Ref. 17); target-heating calculations for  $\eta_{L \rightarrow e} = 10\%$  and 30%.

A reduction in the  $K_\beta/K_\alpha$  ratio is observed with increasing laser energy and decreasing target volume. At the lowest target-energy densities studied ( $\sim 1.5 \times 10^3 \text{ J/mm}^3$ ), laser-generated hot electrons interact with cold target material. When the target energy density is increased to greater than  $1 \times 10^5 \text{ J/mm}^3$ , target heating and thermal ionization suppress  $K_\beta/K_\alpha$ . For target energy densities of  $\sim 5 \times 10^5 \text{ J/mm}^3$ ,  $K_\beta/K_\alpha$  is suppressed to  $40 \pm 4\%$  of the cold-material value.

The experimental trend in  $K_\beta/K_\alpha$  with  $\tau_p = 10$ -ps pulses is in excellent agreement with previous studies that were performed at significantly lower, joule-class laser energies and picosecond-pulse durations.<sup>17</sup> The same rate of change in  $K_\beta/K_\alpha$  is observed with increasing energy density, independent of laser-pulse duration from  $1 \text{ ps} \leq \tau_p \leq 10 \text{ ps}$ . For the parameter space studied, variations in laser spot size, laser intensity, laser prepulse, and angle of incidence do not alter this observation. Scaled for laser energy and target mass, the results from these experiments suggest that the same fraction of laser energy is transferred into K-photon-generating hot electrons, independent of laser-pulse duration.

This interpretation is supported by two-dimensional, cylindrically symmetric target-heating calculations using the implicit-hybrid particle-in-cell code *LSP*.<sup>31</sup> Self-generated fields are included in the model and are calculated self-consistently. Target charging and heating in the calculations were produced by a hot-electron population that had an exponential energy distribution, with a temperature of up to several hundred keV, as defined by the ponderomotive scaling<sup>22</sup> and the range of experimental laser irradiation conditions. Spatial and temporal heating variations are accounted for when determining K-photon emission, with the emission probability calculated using the local temperature at the time of emission. The Thomas-Fermi equation-of-state model used was appropriate for the range of temperatures achieved in this experiment.

The calculated values for  $K_\beta/K_\alpha$  as a function of increasing energy density are shown in Fig. 124.15. Calculations were performed assuming  $\eta_{L \rightarrow e} = 10\%$  and  $30\%$ . The target-heating model predicts suppression in  $K_\beta/K_\alpha$  very similar to that observed in the experiment. The thermal electron temperature inferred from the model for different target interactions is shown in Fig. 124.15 (right axis). This temperature represents a measure of the degree of target heating by hot-electron energy deposition and is weighted by the K-photon emission rate. Weighted thermal electron temperatures approaching several hundred electron volts are achieved in the smallest-mass tar-

gets. Regions of the target that do not emit K photons could reach higher thermal temperatures.

Strong reduction of  $K_\beta/K_\alpha$  in the calculations support the interpretation that in hot Cu-foil targets, thermal ionization causes K-photon suppression with hot-electron refluxing being the dominant energy transfer mechanism. An energy-coupling efficiency to hot electrons of  $\eta_{L \rightarrow e} = 20 \pm 10\%$  reproduces the majority of the experimental  $\tau_p = 10$ -ps data. This range of  $\eta_{L \rightarrow e}$  is in good agreement with previous  $\tau_p = 1$ -ps studies at similar laser intensities.<sup>16,17</sup>

Calculations indicate that around 5% of the hot-electron energy is ohmically dissipated in the high-temperature, low-resistivity plasma. The calculations do not account for fast-proton acceleration by sheath fields at the target surface, with previous measurements indicating 1% to 2% energy-transfer efficiencies to protons.<sup>32,33</sup> The inferred value for  $\eta_{L \rightarrow e}$  therefore represents a lower bound on the energy-conversion efficiency into hot electrons that is required to generate the experimentally observed K-photon emission.

In summary, thin-foil targets have been heated with hot electrons generated by a  $\tau_p = 10$ -ps pulse at focused intensities of  $I > 10^{18} \text{ W/cm}^2$ . K-photon spectroscopy and target-heating calculations show an energy-coupling efficiency into hot electrons of  $\eta_{L \rightarrow e} \sim 20\%$  with laser powers from  $1 \text{ TW} \leq P_L \leq 210 \text{ TW}$ . These measurements are in excellent agreement with previous  $\tau_p = 1$ -ps data at similar laser intensities, demonstrating that the energy-conversion efficiency into hot electrons is independent of laser-pulse duration from  $1 \text{ ps} \leq \tau_p \leq 10 \text{ ps}$ . Ultrafast x-ray streak camera measurements suggest that laser energy is coupled into hot electrons over the entire duration of the incident laser drive. These results are important for the understanding of hot-electron generation in long-pulse, high-intensity laser-solid interactions, such as those found in fast-ignition and high-brightness x-ray-generation experiments.

#### ACKNOWLEDGMENT

This work was supported by the U.S. Department of Energy Office of Inertial Confinement Fusion under Cooperative Agreement Nos. DE-FC52-08NA28302 and DE-FC02-04ER54789, the University of Rochester, and the New York State Energy Research and Development Authority. The support of DOE does not constitute an endorsement by DOE of the views expressed in this article.

#### REFERENCES

1. M. I. K. Santala *et al.*, Phys. Rev. Lett. **84**, 1459 (2000).
2. E. L. Clark *et al.*, Phys. Rev. Lett. **84**, 670 (2000).

3. R. A. Snavely, M. H. Key, S. P. Hatchett, T. E. Cowan, M. Roth, T. W. Phillips, M. A. Stoyer, E. A. Henry, T. C. Sangster, M. S. Singh, S. C. Wilks, A. MacKinnon, A. Offenberger, D. M. Pennington, K. Yasuike, A. B. Langdon, B. F. Lasinski, J. Johnson, M. D. Perry, and E. M. Campbell, *Phys. Rev. Lett.* **85**, 2945 (2000).
4. P. K. Patel *et al.*, *Phys. Rev. Lett.* **91**, 125004 (2003).
5. B. A. Remington *et al.*, *Science* **284**, 1488 (1999).
6. M. H. Key, M. D. Cable, T. E. Cowan, K. G. Estabrook, B. A. Hammel, S. P. Hatchett, E. A. Henry, D. E. Hinkel, J. D. Kilkenny, J. A. Koch, W. L. Kruer, A. B. Langdon, B. F. Lasinski, R. W. Lee, B. J. MacGowan, A. MacKinnon, J. D. Moody, M. J. Moran, A. A. Offenberger, D. M. Pennington, M. D. Perry, T. J. Phillips, T. C. Sangster, M. S. Singh, M. A. Stoyer, M. Tabak, G. L. Tietbohl, M. Tsukamoto, K. Wharton, and S. C. Wilks, *Phys. Plasmas* **5**, 1966 (1998).
7. M. Tabak *et al.*, *Phys. Plasmas* **1**, 1626 (1994).
8. D. F. Price *et al.*, *Phys. Rev. Lett.* **75**, 252 (1995).
9. H. Chen, B. Soom, B. Yaakobi, S. Uchida, and D. D. Meyerhofer, *Phys. Rev. Lett.* **70**, 3431 (1993).
10. K. B. Wharton *et al.*, *Phys. Rev. Lett.* **81**, 822 (1998).
11. K. Yasuike *et al.*, *Rev. Sci. Instrum.* **72**, 1236 (2001).
12. S. P. Hatchett, C. G. Brown, T. E. Cowan, E. A. Henry, J. S. Johnson, M. H. Key, J. A. Koch, A. B. Langdon, B. F. Lasinski, R. W. Lee, A. J. MacKinnon, D. M. Pennington, M. D. Perry, T. W. Phillips, M. Roth, T. C. Sangster, M. S. Singh, R. A. Snavely, M. A. Stoyer, S. C. Wilks, and K. Yasuike, *Phys. Plasmas* **7**, 2076 (2000).
13. F. N. Beg *et al.*, *Phys. Plasmas* **4**, 447 (1997).
14. Y. Ping *et al.*, *Phys. Rev. Lett.* **100**, 085004 (2008).
15. W. Theobald, K. Akli, R. Clarke, J. Delettrez, R. R. Freeman, S. Glenzer, J. Green, G. Gregori, R. Heathcote, N. Izumi, J. A. King, J. A. Koch, J. Kuba, K. Lancaster, A. J. MacKinnon, M. Key, C. Mileham, J. Myatt, D. Neely, P. A. Norreys, H.-S. Park, J. Pasley, P. Patel, S. P. Regan, H. Sawada, R. Shepherd, R. Snavely, R. B. Stephens, C. Stoeckl, M. Storm, B. Zhang, and T. C. Sangster, *Phys. Plasmas* **13**, 043102 (2006).
16. J. Myatt, W. Theobald, J. A. Delettrez, C. Stoeckl, M. Storm, T. C. Sangster, A. V. Maximov, and R. W. Short, *Phys. Plasmas* **14**, 056301 (2007).
17. P. M. Nilson, W. Theobald, J. F. Myatt, C. Stoeckl, M. Storm, J. D. Zuegel, R. Betti, D. D. Meyerhofer, and T. C. Sangster, *Phys. Rev. E* **79**, 016406 (2009).
18. L. J. Waxer, D. N. Maywar, J. H. Kelly, T. J. Kessler, B. E. Kruschwitz, S. J. Loucks, R. L. McCrory, D. D. Meyerhofer, S. F. B. Morse, C. Stoeckl, and J. D. Zuegel, *Opt. Photonics News* **16**, 30 (2005).
19. A. G. MacPhee *et al.*, *Phys. Rev. Lett.* **104**, 055002 (2010).
20. F. Perez *et al.*, *Phys. Rev. Lett.* **104**, 085001 (2010).
21. A. J. Kemp, Y. Sentoku, and M. Tabak, *Phys. Rev. Lett.* **101**, 075004 (2008).
22. S. C. Wilks *et al.*, *Phys. Rev. Lett.* **69**, 1383 (1992).
23. K. U. Akli, S. B. Hansen, A. J. Kemp, R. R. Freeman, F. N. Beg, D. C. Clark, S. D. Chen, D. Hey, S. P. Hatchett, K. Highbarger, E. Giraldez, J. S. Green, G. Gregori, K. L. Lancaster, T. Ma, A. J. MacKinnon, P. Norreys, N. Patel, J. Pasley, C. Shearer, R. B. Stephens, C. Stoeckl, M. Storm, W. Theobald, L. D. Van Woerkom, R. Weber, and M. H. Key, *Phys. Rev. Lett.* **100**, 165002 (2008).
24. V. Bagnoud, I. A. Begishev, M. J. Guardalben, J. Puth, and J. D. Zuegel, *Opt. Lett.* **30**, 1843 (2005).
25. V. Bagnoud, J. D. Zuegel, N. Forget, and C. Le Blanc, *Opt. Express* **15**, 5504 (2007).
26. J. Delettrez, R. Epstein, M. C. Richardson, P. A. Jaanimagi, and B. L. Henke, *Phys. Rev. A* **36**, 3926 (1987).
27. C. Stoeckl, W. Theobald, T. C. Sangster, M. H. Key, P. Patel, B. B. Zhang, R. Clarke, S. Karsch, and P. Norreys, *Rev. Sci. Instrum.* **75**, 3705 (2004).
28. A. Pak *et al.*, *Rev. Sci. Instrum.* **75**, 3747 (2004).
29. C. Stoeckl, W. Theobald, P. A. Jaanimagi, P. Nilson, M. Storm, J. A. Delettrez, R. Epstein, T. C. Sangster, D. Hey, A. J. MacKinnon, H.-S. Park, P. K. Patel, R. Shepherd, J. Green, K. L. Lancaster, and P. A. Norreys, *Bull. Am. Phys. Soc.* **52**, 67 (2007).
30. S. D. Baton *et al.*, *High Energy Density Phys.* **3**, 358 (2007).
31. D. R. Welch *et al.*, *Phys. Plasmas* **13**, 063105 (2006).
32. L. Robson *et al.*, *Nat. Phys.* **3**, 58 (2007).
33. J. Fuchs *et al.*, *Nat. Phys.* **2**, 48 (2006).